Quantum critical paraelectrics and the Casimir effect in time

L. Pálová, P. Chandra, and P. Coleman

Department of Physics and Astronomy, Center for Materials Theory, Rutgers University, Piscataway, New Jersey 08854, USA

We study the quantum paraelectric-ferroelectric transition near a quantum critical point, emphasizing the role of temperature as a "finite-size effect" in time. The influence of temperature near quantum criticality may thus be likened to a temporal Casimir effect. The resulting finite-size scaling approach yields $\frac{1}{T^2}$ behavior of the paraelectric susceptibility (χ) and the scaling form $\chi(\omega, T) = \frac{1}{\omega^2} F(\frac{\omega}{T})$, recovering results previously found by more technical methods. We use a Gaussian theory to illustrate how these temperature dependences emerge from a microscopic approach; we characterize the classical-quantum crossover in χ, and the resulting phase diagram is presented. We also show that coupling to an acoustic phonon at low temperatures (T) is relevant and influences the transition line, possibly resulting in a reentrant quantum ferroelectric phase. Observable consequences of our approach for measurements on specific paraelectric materials at low temperatures are discussed.

I. INTRODUCTION

The role of temperature in the vicinity of a quantum phase transition is distinct from that close to its classical counterpart, where it acts as a tuning parameter. Near a quantum critical point (QCP), temperature provides a low energy cutoff for quantum fluctuations; the associated *finite* time scale is defined through the uncertainty relation $\Delta t \sim \frac{\hbar}{k_B T}$. This same phenomenon manifests itself as a boundary condition in the Feynman path integral; it is in this sense that temperature plays the role of a *finite-size effect in time* at a quantum critical point.[1–5] The interplay between the scale-invariant quantum critical fluctuations and the temporal boundary condition imposed by temperature is reminiscent of the Casimir effect,[6–8] where neutral metallic structures attract each other[9–13] due to zero-point vacuum fluctuations.

In this paper we explore the observable ramifications of temperature as a temporal Casimir effect, applying it to the example of a quantum ferroelectric critical point (QFCP) where detailed interplay between theory and experiment is possible below, at and above the upper critical dimension. Our work is motivated by recent experiments on the quantum paraelectric (QPE) SrTiO$_3$ (STO) where $1/T^2$ behavior is measured in the dielectric susceptibility near the QFCP.[14–16] Here we show how this result is simply obtained using finite-size scaling (FSS) in time; more generally we present similar derivations of several measurable quantities, recovering results that have been previously derived using more technical diagrammatic,[17–20] large N (Ref. 21), and renormalization-group (RG) methods.[22,23] In particular we present a simple interpretation of finite-temperature crossover functions near quantum critical points previously found using ϵ-expansion techniques,[23] and link them to ongoing low-temperature experiments on quantum paraelectric materials. We illustrate these ideas using a Gaussian theory to characterize the domain of influence of the QFCP and we present the full phase diagram. Next we expand upon previous work by tuning away from the QFCP, studying deviations from scaling; here we find that coupling between the soft polarization and long-wavelength acoustic phonon modes is relevant and can lead to a shift of phase boundaries and to a reentrant quantum

ferroelectric (QFE) phase. We end with a discussion of our results and with questions to be pursued in future work.

II. CASIMIR EFFECT IN SPACE AND IN TIME

The Casimir effect is a boundary condition response of the electromagnetic vacuum. The gapless nature of the photon spectrum means that the zero-point electromagnetic fluctuations are scale invariant; the vacuum is literally in a quantum critical state. However, once the boundary conditions are introduced, the system is tuned away from criticality and develops a finite correlation length, ξ. The Coulomb interaction between two charges, the correlation function of the electromagnetic potential inside the cavity, is changed from the vacuum to the cavity as

$$V(q)_{\text{free}} \sim \langle \delta\phi_q \delta\phi_{-q} \rangle = \frac{e^2}{q^2} \to V(q)_{\text{cavity}} \sim \frac{e^2}{q_\perp^2 + \xi^{-2}}, \quad \xi = \frac{a}{\pi}, \tag{1}$$

where the plates have removed field modes and have introduced a finite ξ. In an analogous way, the partition function of a quantum system at finite temperatures is described by a Feynman path integral over the configurations of the fields in Euclidean space time[24] where temperature introduces a cutoff in the temporal direction. In Fig. 1 we present a visual comparison of the Casimir effect in space and in time. In both cases, the finite boundary effects induce the replacement of a continuum of quantum mechanical modes by a discrete spectrum of excitations.

In the quantum paraelectric of interest here, the path integral is taken over the space-time configurations of the polarization field $P(\vec{x}, \tau)$,

$$Z = \sum_{\{P(x,\tau)\}} \exp\left[-\frac{S_E[P]}{\hbar} \right], \tag{2}$$
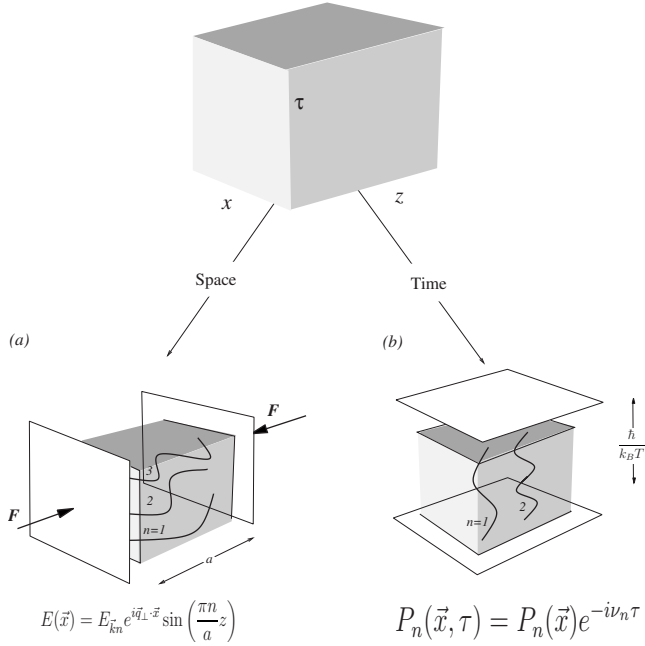
where

FIG. 1. Casimir effect in space and time. (a) Imposition of spatial boundaries on the quantum critical electromagnetic field yields the conventional Casimir effect. (b) Imposition of temporal boundary conditions on a quantum critical paraelectric generates the effect of nonzero temperature.

$$S_E[P] = \int_0^{\hbar/k_B T} d\tau d^3x \mathcal{L}_E[P] \tag{3}$$

and $\mathcal{L}_E[P]$ is the Lagrangian in Euclidean space time. The action per unit time is now the Free energy F of the system (see Table I). The salient point is that finite temperature imposes a *boundary condition in imaginary time* and the allowed configurations of the bosonic quantum fields are periodic in the imaginary time interval $\tau \in [0, \hbar\beta]$ ($\beta \equiv \frac{1}{k_B T}$) so that $\vec{P}(\vec{x}, \tau) = \vec{P}(\vec{x}, \tau + \hbar\beta)$, which permits the quantum fields are thus decomposed in terms of a discrete set of Fourier modes

$$P_n(\vec{x}, \tau) = \sum_{\vec{q},n} P(\vec{q}, i\nu_n) e^{i(\vec{q}\cdot\vec{x} - \nu_n \tau)}, \tag{4}$$

where

$$\nu_n = n\left(\frac{2\pi k_B T}{\hbar}\right) \tag{5}$$

are the discrete Matsubara frequencies; we recall that at $T = 0$ the (imaginary) frequency spectrum is a continuum. The response and correlation functions in (discrete) imaginary frequency

$$\chi_E(\vec{q}, i\nu_n) = \langle P(\vec{q}, i\nu_n) P(-\vec{q}, -i\nu_n)\rangle \tag{6}$$

can be analytically continued to yield the retarded response function

$$\chi_E(\vec{q}, i\nu_n) \rightarrow \chi_E(\vec{q}, \omega) = \chi_E(\vec{q}, z)|_{z=\omega+i\delta}, \tag{7}$$

where ω is a real frequency; for writing convenience we will subsequently drop the E subscript in χ, e.g., $\chi(\vec{q}, \omega) \equiv \chi_E(\vec{q}, \omega)$.

Like the parallel plates in the traditional Casimir effect, temperature removes modes of the field. In this case it is the frequencies not the wave vectors that assume a discrete character, namely,

$$q = (\vec{q}, \omega) \rightarrow (\vec{q}, i\nu_n), \tag{8}$$

where ν_n are defined in Eq. (5).

The Casimir analogy must be used with care. In contrast to the noninteracting nature of the low-energy electromagnetic field, the modes at a typical QCP are interacting. In the conventional Casimir effect, the finite correlation length is induced purely through the discretization of momenta perpendicular to the plates. By contrast, at an interacting QCP, the discretization of Matsubara frequencies imposed by the boundary condition generates the thermal fluctuations in the fields in real time. These are fed back via interactions to generate a temperature-dependent gap in the spectrum and a finite correlation time. Despite the complicated nature of this feedback, provided the underlying system is critical, temperature acting as a boundary condition in time will set the scale of the finite correlation time

$$\xi_\tau = \frac{\hbar}{\kappa k_B T}, \tag{9}$$

where κ is a constant. In cases where the quantum critical physics is universal, such as ferroelectrics in dimensions below $d=3$, we expect the coefficient κ to be also universal and independent of the underlying strength of the mode-mode

TABLE I. Casimir effect and quantum criticality.

	Casimir effect	Finite-temperature effects near quantum criticality
Boundary condition	Space	Time
"S matrix"	$U = e^{-iE\bar{t}/\hbar}$	$Z = e^{-\beta F}$
Path integral	$U = \int D[\phi]\exp[iS[\phi]/\hbar]$	$Z = \int D[P]\exp[-S_E[P]/\hbar]$
Action/time	E	$S_E/\beta\hbar = F$
Time interval	$\bar{t}(\rightarrow \infty)$	$\beta\hbar$
Spatial interval	a	∞
Discrete wave vector/frequency	$q_{zn} = (\pi/a)n$	$\nu_n = (2\pi k_B T/\hbar)n$

coupling. The "temporal confinement" of the fields in imaginary time thus manifests itself as a finite response time in the real-time correlation and response functions.

For the quantum paraelectric at the QFCP, the imaginary time correlation functions are scale invariant,

$$\chi(\vec{q}, i\nu) = \langle P(\vec{q}, i\nu) P(-\vec{q}, -i\nu) \rangle|_{T=0} \sim \frac{1}{\nu^2 + c_s^2 q^2}. \quad (10)$$

At a finite temperature this response function acquires a finite correlation time

$$\chi(\vec{q}, i\nu_n) \sim \frac{1}{\nu_n^2 + c_s^2 q^2 + \xi_\tau^{-2}}, \quad (11)$$

where

$$\xi_\tau^{-2} = 3\gamma_c \{ \langle P^2 \rangle_{T \neq 0} - \langle P^2 \rangle_{T=0} \} \quad (12)$$

is determined by mode-mode interactions, where γ_c is the coupling constant describing the quartic interactions between the modes, to be defined in Sec. IV. We note, as shall be shown explicitly in Sec. IV, that for dimensions d such that $1 < d < 3$, the feedback will be sufficiently strong such that ξ_τ will be *independent* of the coupling constant γ_c; by contrast for $d > 3$ the feedback effects are weak so that there will be a γ_c dependence of ξ_τ. The case $d = d_c^u = 3$ is marginal and will be discussed as a distinct case. At a temperature above a quantum critical point, the energy scale

$$\Delta(T) = \alpha k_B T \quad (13)$$

will set the size of the gap in the phonon dispersion relation. Here $\Delta(T) \sim \hbar \xi_\tau^{-1}$ and $\alpha = O(1)$ is a constant of proportionality.

Reconnecting to our previous discussion, we remark that real-time response functions from expressions like Eq. (11) are obtained by analytic continuation to real frequencies $i\nu_n \to \omega$. Since $\xi_\tau \sim \frac{1}{T}$, the dielectric susceptibility in the approach to the QFCP has the temperature dependence

$$\chi(T) = \chi(q, i\nu_n)|_{q=0, \nu=0} \sim \xi_\tau^2 \propto \frac{1}{T^2}, \quad (14)$$

in contrast to the Curie form ($\chi \sim \frac{1}{T}$) associated with a classical paraelectric; this $1/T^2$ temperature dependence was previously derived from a diagrammatic resummation,[17,18] from analysis of the quantum spherical model[21] and from renormalization-group studies.[22,23] We note that this $1/T^2$ behavior in the dielectric susceptibility of the quantum paraelectric has been observed experimentally.[15,16,25] We summarize in Table I the link between the conventional Casimir effect and finite-temperature behavior in the vicinity of a QCP.

III. FINITE-SIZE SCALING IN TIME

The spatial confinement of order parameter fluctuations near a classical critical point has been studied as a "statistical mechanical Casimir effect," [7,26,27] and here we extend this treatment to study the influence of temperature near a QCP using FSS in imaginary time. This scaling approach is
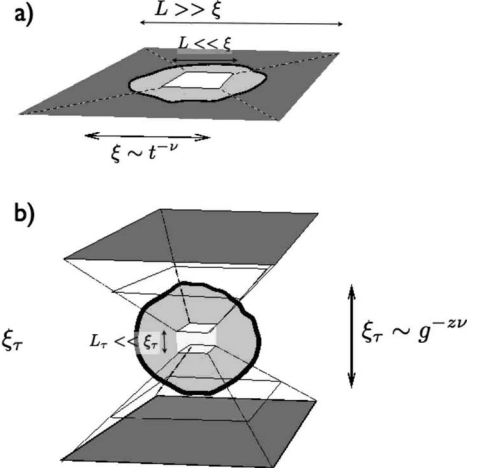

FIG. 2. Schematic of finite-size effects (a) at a classical and at a (b) quantum critical point where the appropriate lengths are defined in the text.

strictly valid in dimensions less than the upper critical dimension. Quantum critical ferroelectrics in $d = 3$ lie at the marginal dimension ($D = d + z = 4$), so the scaling results are valid up to logarithmic corrections, which we will discuss later (Sec. VI); here $z = 1$ refers to a linear dispersion relation, $\omega = c_s q$.

Following the standard FSS procedure,[1,28,29] we impose boundaries on the system near its critical point. For a classical system with tuning parameter $t = \frac{T - T_c}{T_c}$ and correlation length ξ, we confine it in a box of size L and then write the standard FSS scaling form

$$\chi = t^{-\gamma} f\left(\frac{L}{\xi} \right) \quad (15)$$

for the susceptibility.[1,28–30] Similar reasoning can be used when a system is near its QCP. Here temperature is no longer a tuning parameter, this role is taken over by an external tuning field g. Temperature now assumes a new role as a boundary condition in time. Introducing a fixed L_τ [see Fig. 2(b)] associated with a finite T, while replacing $t \to g$, the quantum critical version of Eq. (15) is

$$\chi = g^{-\gamma} \Phi\left(\frac{L_\tau}{\xi_\tau} \right), \quad (16)$$

where g is the tuning parameter. The dispersion relation $\omega = c_s q^z$ yields $[\xi_\tau] = [\xi^z]$; this combined with $\xi \sim g^{-\bar{\nu}}$ leads to $\xi_\tau \sim g^{-z\bar{\nu}}$. We therefore write

$$\chi = g^{-\gamma} \Phi\left(\frac{L_\tau}{g^{-z\bar{\nu}}} \right), \quad (17)$$

where $\Phi(x) \sim x^p$ is a crossover function where p is determined by the limiting values of $\Phi(x)$; when $x \to 0$, we expect $\chi = \chi(L_\tau)$, whereas we should recover the zero-temperature result ($\chi \sim g^{-\gamma}$) when $x \to \infty$. Therefore we obtain
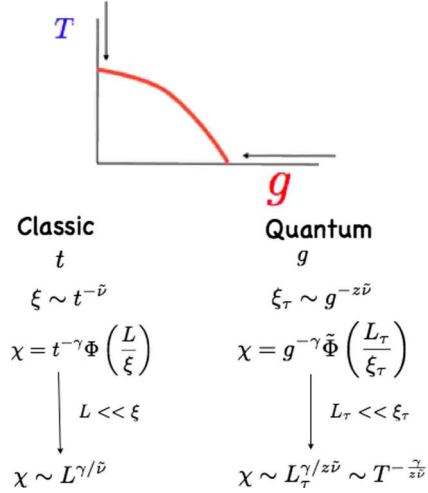
Classical to Quantum Scaling

FIG. 3. (Color online) Overview of the finite-size scaling at classical and quantum critical points; here $\tilde{\nu}$ is the exponent associated with the spatial correlation length since ν has already been used in the text as a frequency.

$$\chi \sim g^{-\gamma}\left(\frac{L_\tau}{g^{-z\tilde{\nu}}}\right)^{\gamma/z\tilde{\nu}} \sim L_\tau^{\gamma/z\tilde{\nu}} \sim T^{-\gamma/z\tilde{\nu}} \qquad (18)$$

and the temperature dependence ($L_\tau \propto 1/T$) emerges naturally from FSS arguments. Therefore a ($T=0$) quantum critical point can influence thermodynamic properties of a system at finite T just as a finite-size system displays aspects of classical critical phenomena despite its spatial constraints. A schematic overview of the finite-size scaling arguments we have presented here is displayed in Fig. 3.

The FSS approach can also yield the T dependences of the specific heat and the polarization of a quantum critical paraelectric. At a finite-temperature phase transition, to obtain the specific-heat capacity of a finite-size box with $L \ll \xi$, we write $f \sim t^{2-\alpha}F(L/\xi) \sim t^{2-\alpha}(\frac{L}{t^{-\nu}})^{-(2-\alpha)/\nu} \sim L^{-(2-\alpha)/\nu}$. In a similar spirit, applying the quantum FSS analogies ($L \rightarrow L_\tau, t \rightarrow g, \xi \rightarrow \xi_\tau^z = g^{-z\tilde{\nu}}$), we obtain

$$f_{qm}(L_\tau) \sim g^{2-\alpha}\left(\frac{L_\tau}{g^{-z\tilde{\nu}}}\right)^{-(2-\alpha)/z\tilde{\nu}} \sim L_\tau^{-2-\alpha/z\tilde{\nu}} \sim T^{2-\alpha/z\tilde{\nu}} \quad (19)$$

so that the T-dependent specific heat is

$$c_v(T) = T\partial^2 f_{qm}/\partial T^2 \sim T^{2-\alpha/z\tilde{\nu}-1} \qquad (20)$$

in the vicinity of a QCP. Similarly the T dependence of the polarization is $P(T) \sim T^{\beta/z\tilde{\nu}}$ and we note that $P(E) = \partial f_{qm}/\partial E|_{g=0} \sim E^{1/\delta}$ is T independent, since finite-temperature scaling does not affect field behavior.

Simple scaling relations at classical and quantum criticality are summarized in Fig. 3. The key notion is that at a QCP, finite T effects correspond to the limit $L_\tau \ll \xi_\tau$; in this case L_τ becomes the effective correlation length in time, and the T dependences follow. We note that we expect this finite-size

TABLE II. Observables for a $D=4$ QPE in the vicinity of a QFCP.

Observable	T dependences ($g=0$)	g dependences ($T=0$)
Polarization	$P \sim T^1$	$P \sim g^{1/2}$
Susceptibility	$\chi \sim T^{-2}$	$\chi \sim g^{-1}$
	$P \sim E^{1/3}$	
	$\chi(\omega,T)=(1/\omega^2)F(\omega/T)$	

approach to work for dimensions $d < d_c^u$ where there will be logarithmic corrections to scaling in the upper critical dimension d_c^u.

Let us now be more specific with exponents for the quantum paraelectric case. At criticality the observed T dependence of the paraelectric susceptibility (χ) can be found by a soft-mode analysis,[31,32] and therefore the exponents for the quantum paraelectric are those of the quantum spherical model.[21] For the case of interest ($D=d+z=3+1=4$), the quantum spherical model has exponents $\tilde{\nu}=1/(D-2)=1/2$ and $\gamma=2/(D-2)=1$, so that $\gamma_{th}=\frac{\gamma}{z\tilde{\nu}}=2$ and we recover the $\chi^{-1} \sim T^2$ scaling found earlier. Other specific T dependences are displayed in Table II. For $d=3$, we have $g \sim T^2$; this relation was experimentally observed[14,33] in STO. Finally we note that the FSS that we have discussed suggests the "$\frac{\omega}{T}$" scaling form

$$\chi(\omega,T) = \frac{1}{\omega^2}F\left(\frac{\omega}{T}\right) \qquad (21)$$

that is similar to that observed in other systems at quantum criticality;[34,35] this was previously derived by more technical methods.[23] Predictions for experiment are summarized in Table II. We note that since we are in the upper critical dimension, there will be logarithmic corrections to this scaling but we do not expect these to be experimentally important for the temperature dependences described here; however they will be considered later in the paper (Sec. VI).

IV. GAUSSIAN THEORY: ILLUSTRATION OF TEMPERATURE AS A BOUNDARY EFFECT

A. Gap equation

In this section we use the self-consistent Gaussian theory to illustrate how the $\chi(T)$ found via FSS in time appears from a more microscopic approach; we also study the crossover behavior between the classical and the quantum critical points. This approach is equivalent to the self-consistent one-loop approximation[36] that is used in the context of metallic magnetism.

The soft-mode treatment has been described extensively elsewhere;[31,32,36] here we briefly outline the derivation of the gap equation. The Lagrangian in Euclidean space time, $\mathcal{L}_E$ in Eq. (3), for displacive ferroelectrics is the ϕ^4 model:
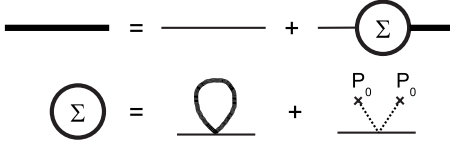
FIG. 4. Diagrammatic representation of (a) the Dyson equation and (b) the Gaussian self-energy where $P_0=0$ in the paraelectric state (and is finite in the ferroelectric phase).

$$\mathcal{L}_E \to \frac{1}{2}[(\partial_\tau P)^2 + (\nabla P)^2 + rP^2] + \frac{\gamma_c}{4}P^4, \qquad (22)$$

which determines the partition function. Notice that in writing Eq. (22), we have chosen rescaled units in which the characteristic speed of the soft mode $c_s=1$. In a self-consistent Hartree theory, interaction feedback is introduced via its renormalization of quadratic terms; this procedure is equivalent to replacing $\mathcal{L}_E$ by the Gaussian Lagrangian

$$\mathcal{L}_G = \frac{1}{2}P[-\partial_\tau^2 - \nabla^2 + r + \Sigma]P, \qquad (23)$$

where

$$\Sigma = 3\gamma_c\langle P^2\rangle \qquad (24)$$

is the Hartree self-energy (see Fig. 4). We note that this mode-mode coupling theory is exact for the "spherical model" generalization of ϕ^4 theory in which the order parameter has N components and N is taken to infinity.

The Green's function can now be determined from Dyson's equation, shown diagrammatically in Fig. 4, and takes the form

$$G(q) \equiv G(\vec{q}, i\nu_n) = [(i\nu_n)^2 - q^2 - r - \Sigma]^{-1}, \qquad (25)$$

so the action is diagonalized in this basis. The poles of $G(\vec{q}, \omega)$ determine the dispersion relation ω_q for the displacive polarization modes

$$\omega_q^2 = q^2 + \Delta^2, \qquad (26)$$

where here we have introduced the gap function

$$\Delta^2(r,T) = r + \Sigma(r,T). \qquad (27)$$

This quantity vanishes at both quantum and classical critical points where there are scale-free (gapless) fluctuations. At the quantum critical point where $T_c=0$, $\Delta(r_c,0)=r_c + \Sigma(r_c, T=0)$, so that we can eliminate $r_c = -\Sigma(r_c, T=0)$, to obtain

$$\Delta^2(r,T) = \Omega_0^2 + [\Sigma(r,T) - \Sigma(r_c, 0)], \qquad (28)$$

where $\Omega_0^2 = (r - r_c) = g$.

The amplitude of the polarization fluctuations is given by

$$\langle P^2\rangle = -G(0,0) = -\frac{1}{\beta V}\sum_q G(q)e^{iqx}|_{x=0}, \qquad (29)$$

so the self-consistency (24) condition $\Sigma = 3\gamma_c\langle P^2\rangle$ can now be written

$$\Sigma(r,T) = (-3\gamma_c)T\sum_n \int \frac{d^d q}{(2\pi)^d} G(q, i\nu_n), \qquad (30)$$

where $\Sigma(r,T)$ is the temperature-dependent self-energy. By converting the discrete Matsubara summation to a contour integral, deformed around the poles $z = \pm\omega(q)$ in the dispersion relation, we can convert this expression to the form

$$\Sigma(r,T) = 3\gamma_c \int \frac{d^d q}{(2\pi)^d} \frac{\left[n_B(\omega_q) + \frac{1}{2}\right]}{\omega_q}, \qquad (31)$$

where we denote $n_B(\omega) \equiv n_B(\omega, \beta) = 1/(e^{\beta\omega} - 1)$. At the quantum critical point ($r=r_c$ and $T=0$), we have $\omega_q = q$ and $n(\omega_q) = 0$ so that

$$\Sigma(r_c, 0) = 3\gamma_c \int \frac{d^d q}{(2\pi)^d} \frac{1}{2q}, \qquad (32)$$

and using Eq. (28), we can write the gap function as

$$\Delta^2 = \Omega_0^2 + 3\gamma_c \int \frac{d^d q}{(2\pi)^d}\left(\frac{\left[n_B(\omega_q) + \frac{1}{2}\right]}{\omega_q} - \frac{1}{2q}\right),$$

$$\omega_q = \sqrt{q^2 + \Delta^2}. \qquad (33)$$

B. T dependence of the gap at the QCP

In the paraelectric phases, we can use the temperature-dependent gap to determine the dielectric susceptibility χ. Writing

$$\chi = \chi(q,\omega)|_{\vec{q},\omega=0} = \langle P(q)P(-q)\rangle|_{q=0} = -G(\vec{q},\omega)|_{\vec{q},\omega=0}, \qquad (34)$$

we use Eqs. (25) and (27) to express it as

$$\chi^{-1}(r,T) = \Delta^2(r,T). \qquad (35)$$

At the quantum critical point $\Omega_0^2 = 0$, so the gap Eq. (33) becomes

$$\Delta^2(r_c, T) = 3\gamma_c \int_0^{q<q_{max}} \frac{d^d q}{(2\pi)^d}\left\{\frac{\left[n_B(\omega_q) + \frac{1}{2}\right]}{\sqrt{q^2 + \Delta^2}} - \frac{1}{2q}\right\}, \qquad (36)$$

where we have inputted the dispersion relation (26) for ω_q in Eq. (36). We notice that both thermal and quantum fluctuations contribute to this expression.

Even though the mean-field gap equation is only formally exact in the spherical mean-field limit, it is sufficient to illustrate the qualitative influence of T on the gap at the QCP. In order to explore the cutoff dependence of Eq. (36), we note that in the ultraviolet limit of interest, the last two terms can be expressed as

$$\frac{1}{2}\left\{\frac{1}{\omega_q}-\frac{1}{q}\right\}=-\frac{\Delta^2}{4q^3}, \tag{37}$$

where there is complete cancellation when $\Delta=0$ exactly at the QCP. However just slightly away from it, when Δ is finite, Eq. (37) leads to a q_{max}^{d-3} scaling dependence of the integral in Eq. (36); therefore the cutoff is required to ensure that Eq. (36) is finite in dimensions $d>3$. However, in dimensions $d<3$, this integral is convergent in the ultraviolet and the upper cutoff in Eq. (36) can be entirely removed. Thus, for $d<3$, the only scale in the problem is temperature itself. The integral is also convergent in the infrared provided $d>1$. The spatial dimensions $d=1$ and $d=3$ correspond to space time dimensions $D=d+1=2$ and $D=d+1=4$, which are the well-known lower and upper critical dimensions of the ϕ^4 theory. This provides us with a dimensional window $1<d<3$ where inverse temperature acts as a cutoff in time. In this range, the temperature dependence of the gap

$$\Delta(T)=\alpha_d T \tag{38}$$

is independent of the strength of the coupling constant γ_c and the cutoff, a feature that can be illustrated already within mode-coupling theory. Recalling that $\Delta(T)=\frac{\alpha}{L_\tau}$ and $\alpha\equiv\alpha_d$ [see Eq. (13) and Fig. 1], we note that confirmation of Eq. (38) is consistent with our earlier discussion [see after Eq. (12)] that ξ_τ is independent of coupling constant; in this dimensional window, temperature is a boundary effect in (imaginary) time and is the only temporal scale in the problem.

In order to calculate α_d, we rewrite the gap equation at criticality as

$$\frac{\Delta^2}{T^2}=\alpha^2=\frac{3\gamma_c}{T^2}\Gamma_d\int_0^\infty\frac{q^{d-1}dq}{(2\pi)^d}\left\{\frac{\left[n_B(\omega_q)+\frac{1}{2}\right]}{\omega_q}-\frac{1}{2q}\right\}, \tag{39}$$

where $\Gamma_d q^{d-1}dq$ ($\Gamma_d=\frac{2\pi^{d/2}}{\Gamma(d/2)}$) is the d-dimensional volume measure. Rescaling $\Delta=\alpha_d T$ and $q=uT$, we obtain

$$F_d[\alpha]=T^{3-d}\alpha_d^2/\gamma_c, \tag{40}$$

where

$$F_d[\alpha]=\frac{3}{(2\sqrt{\pi})^d\Gamma(d/2)}\int_0^\infty u^{d-1}du\left\{\frac{\coth\left(\frac{1}{2}\sqrt{u^2+\alpha^2}\right)}{\sqrt{u^2+\alpha^2}}-\frac{1}{u}\right\}. \tag{41}$$

For $d<3$, the temperature prefactor on the right-hand side of Eq. (40) vanishes $T\to0$, so a consistent solution requires α_d to satisfy

$$F_d[\alpha_d]=0. \tag{42}$$

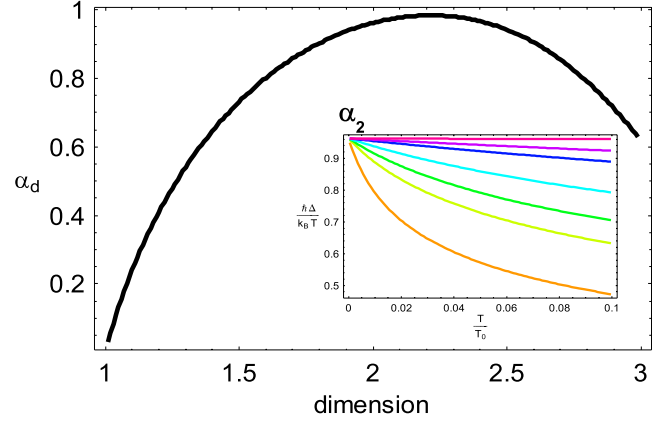At a small finite temperature, we can expand around $\alpha=\alpha_d+\delta\alpha(T)$ to obtain

FIG. 5. (Color online) Dependence of $\alpha_d(T\to0)$ on dimensionality d. Inset: T dependence of Δ/T for $d=2$ and couplings in the range $0.01<\frac{\gamma_c(d=2)}{q_{max}}<5.0$; here T_0 is the temperature scale where $\xi\sim a$ and we note that $\lim_{T\to0}\alpha_2$ is independent of γ_c.

$$\Delta(T)=\alpha_d T+\left(\frac{\alpha_d^2}{\gamma_c F'[\alpha_d]}\right)T^{4-d}. \tag{43}$$

Thus in dimensions $d<3$, the dominant low-temperature behavior is independent of γ_c, the strength of the mode-mode coupling, which enters into the subleading temperature dependence. For $d=3$, the linear coefficient of $\Delta(T)$ depends on γ_c, becoming independent of γ_c in the limit that $\gamma_c\to\infty$; here we have neglected logarithmic corrections in α. We remark that here we are presenting and expanding a previous analysis,[21] noting that the γ_c independence of α for $d\leq3$ can be understood via the insight that temperature is a boundary effect in time. As an aside, we note that there is a discrepancy between our result for α_3 (finite) and that found from ϵ calculations[23] (zero) which may be attributed to an order of limits issue ($\epsilon\to0$ and $N\to\infty$).

In Fig. 5 we display the dependence of α_d on dimensionality $1<d<3$. We notice that α_d goes to zero as the dimension approaches the lower critical dimension $d_c^l=1$. The temperature dependence of the gap in two dimensions is shown in the inset of Fig. 5, where we see that $\lim_{T\to0}\alpha_2\equiv0.96$ is the same for all couplings. According to Eqs. (40) and (41), we write $\alpha_3^2=\gamma_c F_3[\alpha]$ and solve for α_3 in the limit of upper cutoff $u_{max}=q_{max}/T\equiv2\pi T_0/T\gg\alpha_3$,

$$\alpha_3(T,\gamma_c)\sim\sqrt{\frac{\gamma_c}{1+\gamma_c\left(\frac{3}{8\pi^2}\right)\ln\left(\frac{4\pi T_0}{T}\right)}}, \tag{44}$$

where again we do not consider logarithmic corrections to α_3. In the limit of strong coupling, $\alpha_3\sim[\ln(\frac{4\pi T_0}{T})]^{-1/2}$ is γ_c independent. For weak coupling, the situation relevant here, α_3 is indeed a function of γ_c but remains independent of temperature so that $\Delta\sim T$ according to Eq. (38); temperature dependences derived here should therefore be in agreement with those found from a scaling perspective whenever direct comparison is possible.

C. Temperature-dependent dielectric susceptibility

To provide an explicit illustration of the above calculations, we now use Eqs. (33) and (35) to numerically determine the temperature-dependent paraelectric susceptibility in the approach to the quantum critical point (QCP) in $d=3$. We obtain $\chi^{-1}(T)=\Delta^2 \sim T^2$ for the approach $r=r_c$ in agreement with previous results and discussion. We note that a similar analysis in the vicinity of the classical phase transition leads to the expected Curie susceptibility $[\chi^{-1}(T\rightarrow T_c^+\gg 0)\sim T]$ since in this (high) temperature regime the Bose function in Eq. (36) scales as $\frac{T}{\omega}$. We also remark that if we assume that $\omega \equiv \tilde{\omega}_0$ with no q dependence then we recover the Barrett[37] expression $\chi^{-1}\sim A+B\coth\frac{\hbar\tilde{\omega}_0}{k_B T}$; because the dispersion is constant and q independent this approach is not applicable near quantum criticality where the gap vanishes and the q dependence becomes important.

One more point needs to be considered before we proceed with our self-consistent Hartree theory. In the self-consistent Hartree theory (SCHT) of the ferroelectric phase, the polarization field P_0 acquires a nonzero value. P_0 enters the Lagrangian $\mathcal{L}_E$ in Eq. (22) as $P=P_0+\delta P$, where δP are fluctuations of the polarization field around its mean value, P_0 ($P_0=0$ in the paraelectric phase). The self-energy (24) becomes

$$\Sigma = 3\gamma_c\langle P^2\rangle = 3\gamma_c(P_0^2+\langle\delta P^2\rangle) \qquad (45)$$

as indicated diagrammatically in Fig. 4. The equilibrium value P_0 is easily obtained by introducing an electric field into the Lagrangian by replacing $\mathcal{L}_E\rightarrow\mathcal{L}_E+E\cdot P$, then seeking the stationary point $\delta S/\delta P_0=0$ which gives $\langle rP_0 +3\gamma_c\delta P^2 P_0+\gamma_c P_0^3-E\rangle=0$, or

$$r+\Sigma-2\gamma_c P_0^2=\frac{E}{P_0}=0 \qquad (46)$$

at zero electric field. According to Eq. (27), $\Delta^2(r,T)=r +\Sigma(r,T)$, so that the spectral gap in the ferroelectric phase is

$$\Delta_f^2(r,T)=2\gamma_c P_0^2(r,T)>0. \qquad (47)$$

In Fig. 6(a) we plot the calculated temperature-dependent spectral gap $\Delta(r,T)$ for three different values of r as indicated in its schematic inset. As expected, for Eq. (2) the spectral gap closes exactly at $T=0$ leading to a linear dispersion relation, $\omega=q$ at the QCP. We note that in the QPE, Δ (or χ^{-1}) is constant. In the QFE again Δ is constant; though there exists a classical paraelectric-ferroelectric transition at $T=T_c$ where $\chi^{-1}\sim(T-T_c)$. The static dielectric susceptibility in the vicinity of the QCP (low T) is presented in the same three r regimes in Fig. 6(b) where we see that in the QPE regime $\chi(T\rightarrow 0)$ saturates, at the QCP $\chi(T)\sim T^{-2}$ and diverges as $T\rightarrow 0$. In the QFE, the susceptibility also saturates at low temperatures, though the Curie law is recovered in the vicinity of the classical transition at $T=T_c$.

Figure 7 shows the phase diagram that results from the self-consistent Hartree theory. This figure serves to emphasize how the strictly zero-temperature QCP gives rise to a quadratic power-law dependence of the inverse susceptibility on temperature over a substantial region of the $T-g$ phase diagram.
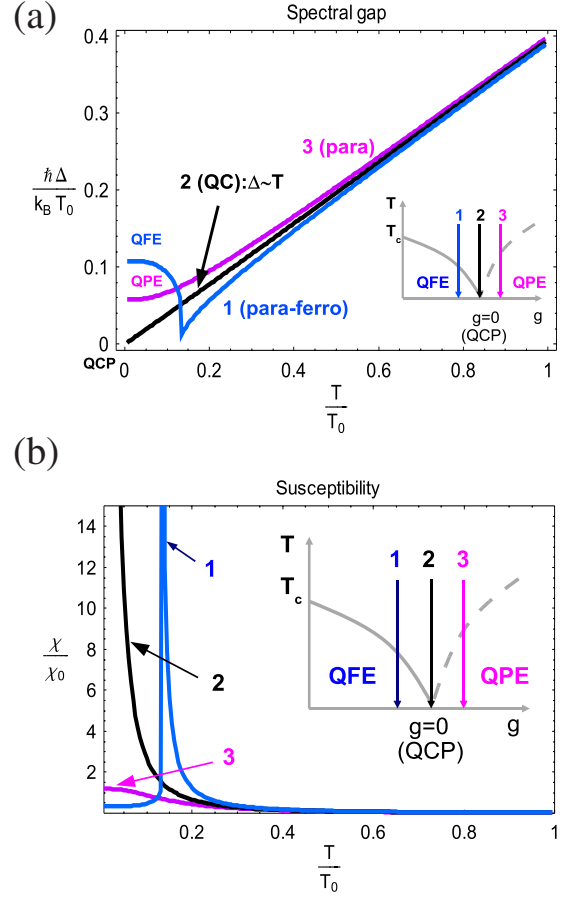

FIG. 6. (Color online) Temperature dependence of the (a) spectral gap and (b) the dielectric susceptibility for three temperature scans defined in the schematic inset; here $g=r-r_c$.

The crossover temperature, T_0, between Curie $(\chi^{-1}\sim T)$ and quantum critical $(\chi^{-1}\sim T^2)$ behavior in the susceptibility is defined by the expression

$$T_0\approx\frac{\hbar\omega_0}{2\pi k_B}, \qquad (48)$$

where $\omega_0=\frac{c_s}{a}$ is the characteristic soft-mode frequency, c_s is the soft-mode velocity, and a is the lattice spacing. Here we have assumed a simple band structure $\omega(q)=\omega_0\sin qa$ such that $c_s=\frac{d\omega}{dq}\big|_{q=0}=(\omega_0 a)\cos qa\big|_{q=0}$ so that $\omega_0=\frac{c_s}{a}$ as stated above. The factor of 2π in the denominator of Eq. (48) results from the observation that the separation of the poles of the Bose and Fermi functions in the complex frequency plane is $\Delta\nu_n=2\pi k_B T$, which sets the natural conversion factor between temperature and frequency to be $2\pi k_B$. T_0 also corresponds to the temperature when the correlation length is comparable to the lattice constant $(\xi\sim a)$; here the correlation length $\xi\equiv\frac{c_s}{\Omega_0}\sim g^{-1/2}$ [see Eq. (17)]. Neutron-scattering measurements[38] of the dispersion relation indicate that the soft-mode velocity in STO is $c_s\approx 10^4$ m/s and the lattice constant has been measured[39] to be $a_{STO}=3.9\times 10^{-10}$ m; therefore $T_0\approx 30$ K. We note that with O^{18} substitution, the ambient pressure Curie temperature[14] is $T_c\sim 25$ K. Using the values of c_s and a_{STO} from above, we get $\omega_0\approx 2.6$

Quantum Phase Diagram

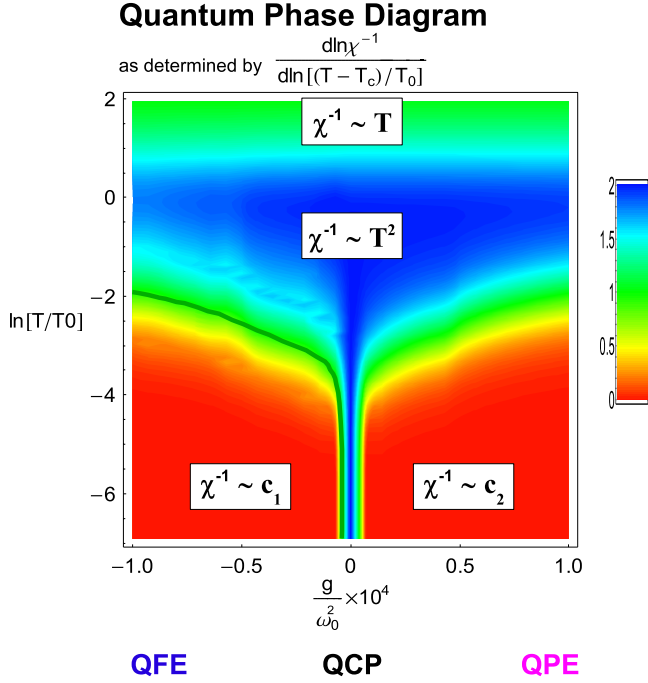as determined by $\dfrac{d\ln \chi^{-1}}{d\ln\left[(T - T_c)/T_0\right]}$

FIG. 7. (Color online) T-g phase diagram as determined by a self-consistent analysis of the dielectric susceptibilty. The power-law exponents are depicted in different colors via the function $\frac{d\ln \chi^{-1}}{d\ln(T-T_c)/T_0}$. This expression selects the exponent 2 (blue region) for $\chi^{-1} \sim T^2$ ($T_c \equiv 0$ for QCP), exponent 1 (green region) for classical Curie behavior $\chi^{-1} \sim (T - T_c)$, and exponent 0 (red region) for a constant susceptibility.

$\times 10^{13}$ Hz in SrTiO$_3$. The typical frequency $\Omega_0 = g^{1/2}$ (spectral gap at zero temperature) at which one observes the change in behavior in the dielectric susceptibility (exponent 2 region) is thus from Fig. 7, $\Omega_0 \approx 10^{-2}$ $\omega_0 = 2.6 \times 10^{11}$ Hz. Indeed, Raman scattering on ferroelectric SrTi^{18}O$_3$ (T_c =25 K) shows that the zero-temperature Raman shift[40] is about 10 cm^{-1} which translates into $\Omega_0 \approx 3 \times 10^{11}$ Hz, in good agreement with our calculation.

V. COUPLING TO LONG-WAVELENGTH ACOUSTIC MODES

A. Overview

In a conventional solid, broken translational symmetry leads to three acoustic Goldstone modes. At a ferroelectric QCP, these three modes are supplemented by one or more optical zero modes. This coexistence of acoustic and optic zero modes is a unique property of the ferroelectric QCP, and in this section we examine how their interaction influences observable properties.

The gap of the optical modes in a ferroelectric is sensitive to the dimensions of the unit cell and couples linearly to the strain field. This leads to an inevitable coupling between the critical optical mode and the long-wavelength acoustic phonons that must be considered. To address this issue, we consider the effect of a coupling η between the soft polarization and the strain field created by a single long-wavelength acoustic phonon mode. Softening of the polar

transverse optic (TO) mode near the QCP enhances the effect of this coupling. Using dimensional analysis we find that the coupling between the TO and LA mode is marginally relevant in the physically important dimension $d=3$, and thus cannot be ignored. The main result of the analysis is that the acoustic phonons act to soften and reduce the quartic interaction between the optic phonons. Beyond a certain threshold $\eta > \eta_c$, this interaction becomes attractive, leading to the development of a reentrant paraelectric phase at finite temperatures. We note that such a coupling to acoustic phonons has been considered previously,[18] and here we are rederiving and extending prior results in a contemporary framework.

B. Lagrangian and dimensional analysis

We introduce the coupling of the polarization ($P(\vec{x}, \tau)$) and the acoustic phonon ($\phi(\vec{x}, \tau)$) fields as a coupling of the polarization to strain $-\eta \nabla \phi P^2$; we then write the Lagrangian[18] as

$$\mathcal{L}_E[P, \phi] = \mathcal{L}_E[P] + \frac{1}{2}[(\partial_\tau \phi)^2 + \tilde{c}^2(\nabla \phi)^2] - \eta \nabla \phi P^2, \tag{49}$$

where $\mathcal{L}_E[P]$ is our previous Lagrangian without acoustic coupling given in Eq. (22). Here the constant η is the coupling strength to the acoustic phonon; the latter's dynamics is introduced in the bracketed terms of Eq. (49). Since we are using units in which the velocity of the soft optical phonon is one, $\tilde{c} = \frac{c_a}{c_s}$ is the ratio of the acoustic to the soft optical phonon velocities. We will discuss the restoration of dimensional constants in Eq. (49) when we make comparison to experiment in Sec. V F.

We begin with a dimensional analysis of the couplings to assess their relative importance in the physically important dimension $d=3$. In order to do so, we introduce the RG flow by rescaling length, time, momentum, and frequency

$$x' = \frac{x}{\Lambda}, \quad \tau' = \frac{\tau}{\Lambda}, \quad q' = q\Lambda, \quad \nu' = \nu\Lambda, \tag{50}$$

with constant $\Lambda > 1$ representing flow away from the infrared (IR) limit of the QCP, that is flow from small to large momentum and frequency. In terms of the rescaled variables x' and τ', the action (3) with Lagrangian (49) in $d+1$ dimensions becomes

$$\begin{aligned} S[P, \phi] &= \int_0^\beta d\tau \int d^dx \mathcal{L}_E[P, \phi] \\ &= \int_0^{\beta/\Lambda} d\tau' \int d^dx' \Lambda^{d+1}\left\{ \frac{1}{2}\Lambda^{-2}[(\partial_{\tau'} P)^2 + (\nabla' P)^2] \right. \\ &\quad + (\partial_{\tau'}\phi)^2 + (\nabla'\tilde{c}\phi)^2] + \frac{1}{2}\Omega_0^2 P^2 + \frac{1}{4}\gamma_c P^4 \\ &\quad \left. - \eta \Lambda^{-1} \nabla' \phi P^2 \right\}. \end{aligned} \tag{51}$$

We emphasize that we write $\Omega_0^2 = r - r_c$ as the coefficient of the P^2 term in the Lagrangian $L_E[P]$ [Eq. (22)], entering Eq.

(49) in Eq. (51), since our RG flow starts from the QCP ($r = r_c$). Rescaling P, ϕ, Ω_0^2, γ_c and η, so that action (51) assumes its initial form, we write

$$P' = P\Lambda^{d-1/2}, \quad \phi' = \phi\Lambda^{d-1/2}, \quad (\Omega_0^2)' = \Omega_0^2\Lambda^2,$$
$$\gamma_c' = \gamma_c\Lambda^{3-d}, \quad \eta' = \eta\Lambda^{2-d+1/2}, \tag{52}$$

which leads to

$$S[P,\phi] = \int_0^{\beta/\Lambda} d\tau' \int d^dx' \mathcal{L}_E[P',\phi']. \tag{53}$$

Now the fields, the mass term, and the coupling constants flow to new values leaving the action unperturbed. We remark that the upper cutoff in the imaginary time dimension is replaced by infinity as the temperature $T \sim \frac{1}{\beta}$ approaches zero.

Analyzing the RG expressions in Eq. (52), we find that the Ω_0^2 term grows as we flow away from the QCP IR limit; therefore it is a relevant perturbation parameter independent of dimension d. This is consistent with the fact that $\Omega_0^2 = r - r_c = g$ *tunes* the system away from the QCP. Similarly we find that couplings γ_c and η grow (relevant) in dimension $d < 3$, decrease (irrelevant) in dimension $d > 3$, and do not change (marginally relevant) in $d = 3$. We see that in this case ($d = 3$) the coupling to acoustic phonons (η') is equally important as the mode-mode coupling (γ_c') and thus has to be included to the Gaussian model.

Let us now briefly summarize what we know about γ_c before we proceed to the discussion of the acoustic coupling η. In Sec. IV B we found that the spectral gap Δ is independent of γ_c for dimensions $1 < d < 3$ in the zero-temperature limit (see Fig. 5). This is in agreement with the above results, where γ_c is a relevant perturbative parameter; more precise analysis[1] shows γ_c flowing to the nontrivial Wilson-Fisher fixed point γ_c^*. Here all the system properties become functions of $\gamma_c^* + \delta\gamma_c \approx \gamma_c^*$, and so are γ_c independent. On the other hand, in dimensions $d > 3$ and $d = 3$, γ_c flows to zero (with logarithmic corrections in the marginal case). In these cases the system properties are functions of $\delta\gamma_c$ and thus are γ_c dependent; we have already seen an example of this behavior in the specific case of the $d = 3$ spectral gap.

C. Gap equation

We are now ready to explore how the system's low-temperature behavior changes in the presence of acoustic phonons in dimension $d = 3$. Let us look first at the LA phonon field ϕ. Following the procedure of Sec. IV A, we find the acoustic Green's function and dispersion relation from Eq. (49) to be

$$D(q) \equiv D(\vec{q}, i\nu_n) = [(i\nu_n)^2 - \tilde{c}^2 q^2]^{-1}, \tag{54}$$

$$\omega_a(q) = \tilde{c}q. \tag{55}$$

We emphasize the P^2 dependency of the interaction term, $-\eta\nabla\phi P^2$, in Lagrangian (49). Therefore it contributes to the polarization self-energy as an additional term inside the brackets of Eq. (23). This second contribution arises due to
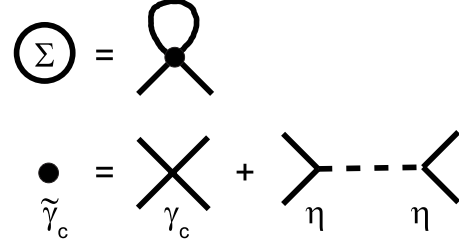

FIG. 8. Diagrammatic representation of the self-energy that includes coupling to both optical and acoustic phonons. Here $\tilde{\gamma}_c$ is the renormalized coupling, including the exchange of an acoustic phonon.

nonzero second-order perturbation and is schematically shown in Fig. 8, where the solid line represents the soft polarization TO Green's function (25) and the dashed line represents the LA Green's function (54). We note that the interaction represented by a *dot* in the self-energy consists of a contribution each from the coupling γ_c and η. Thus we can write the polarization self-energy Σ as a sum of these two terms,

$$\Sigma(r,T) = \Sigma_{\gamma_c}(r,T) + \Sigma_\eta(r,T) = (-3\gamma_c)T\sum_n \int \frac{d^3q}{(2\pi)^3}G(q,i\nu_n)$$
$$+ 4\eta^2 T\sum_n \int \frac{d^3q}{(2\pi)^3}q^2 G(q,i\nu_n)D(q,i\nu_n), \tag{56}$$

where Σ_{γ_c} is the Hartree self-energy (30) previously calculated in Sec. IV A. We remark that the q^2 term in the integral for Σ_η arises due to form of the interaction ($\nabla\phi$). Converting the Matsubara summation to a contour integral, deformed around the poles $z_p = \pm\omega_p(q)$ and $z_a = \pm\omega_a(q)$ in the dispersion relations of the polarization (26) and acoustic phonon (55) modes, respectively, we can rewrite Σ_η in the form[18]

$$\Sigma_\eta(r,T) = -4\eta^2 \int \frac{d^3q}{(2\pi)^3}q^2 \left\{ \frac{\left\{ n_B[\omega_p(q)] + \frac{1}{2}\right\}}{\omega_p[\omega_a^2 - \omega_p^2]} + \frac{\left\{ n_B[\omega_a(q)] + \frac{1}{2}\right\}}{\omega_a[\omega_p^2 - \omega_a^2]} \right\}. \tag{57}$$

At the quantum critical point, where $r = r_c$ and $T = 0$, the dispersion $\omega_p(q) = q$ and $n_B(\omega_p) = n_B(\omega_a) = 0$ so that

$$\Sigma_\eta(r_c, 0) = -4\eta^2 \int \frac{d^3q}{(2\pi)^3}\frac{1}{2\tilde{c}(\tilde{c}+1)q}. \tag{58}$$

Using Eq. (28), we write the gap function (as in Sec. IV A) as

$$\Delta^2 = \Omega_0^2 + \Delta_{\gamma_c}^2 + \Delta_\eta^2,$$

$$\Delta_{\gamma_c}^2 = 3\gamma_c \int \frac{d^3q}{(2\pi)^3}\left(\frac{\left\{ n_B[\omega_p(q)] + \frac{1}{2}\right\}}{\omega_p} - \frac{1}{2q} \right),$$
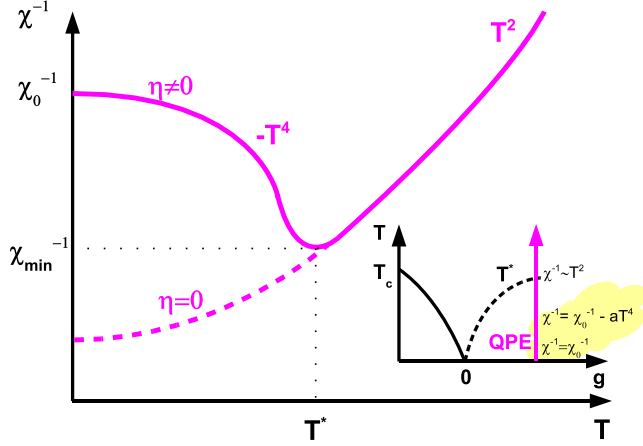
FIG. 9. (Color online) Schematic temperature dependence of the static dielectric susceptibility where coupling to a long-wavelength acoustic phonon is included in the calculation; inset indicates phase trajectory and region of corrections due to acoustic coupling deep in the QPE phase (yellow).

$$\Delta_\eta^2 = -4\eta^2 \int \frac{d^3q}{(2\pi)^3} q^2 \left(\frac{\left\{ n_B[\omega_p(q)] + \frac{1}{2} \right\}}{\omega_p[\omega_a^2 - \omega_p^2]} \right.$$
$$\left. + \frac{\left\{ n_B[\omega_a(q)] + \frac{1}{2} \right\}}{\omega_a[\omega_p^2 - \omega_a^2]} - \frac{1}{2\tilde{c}[\tilde{c} + 1]q^3} \right), \qquad (59)$$

where $\Delta_{\gamma_c}^2$ has been already defined in Eq. (33).

We emphasize that the γ_c and η terms in Eq. (59) have opposite signs in their contribution to the spectral gap Δ. The negative coefficient of η^2 reflects the fact that it emerges from second-order perturbation theory; physically it is due to thermally enhanced virtual excitations caused by coupling between polarization TO and LA phonon modes.

D. Deep in the quantum paraelectric phase

Let us first explore the effect of the acoustic coupling η deep in the QPE region of the phase diagram (see inset of Fig. 9). Here $g \gg 0$ and $\Delta \gg T \approx 0$. In this regime, we write

$$\chi^{-1} = \Delta^2 = \Omega_0^2 + D(\Delta) - A(\eta)\frac{T^4}{\Delta^2}, \qquad (60)$$

with

$$A(\eta) = \frac{4\eta^2}{\tilde{c}} \int \frac{d^3u}{(2\pi)^3} u n_B(\tilde{c}u), \qquad (61)$$

where derivations of $A(\eta)$ and $D(\Delta)$ are presented in Appendix A; for our purposes, the key point is to note that $\lim_{\Delta \to 0} D(\Delta) = 0$. Setting $A(\eta) \sim \eta^2 = 0$, we recover a constant expression for χ as a function of temperature in the QPE phase consistent with our previous derivations from Sec. IV. For $\eta \neq 0$, the dielectric susceptibility acquires different low-temperature behavior. The quartic temperature term in Eq. (60), $-A(\eta)\frac{T^4}{\Delta^2}$, drives the inverse susceptibility at low tem-

peratures; such a "bump" in the susceptibility (or "well" in the inverse susceptibility, see Fig. 9) due to acoustic phonon coupling has been considered previously.[18] It is then natural to inquire whether a finite η could eventually drive the inverse susceptibility to zero (or negative) values. Here we show that this is not the case. We start by looking for a solution of Eq. (60) with $\chi^{-1} = \Delta^2 = 0$ and show that such a solution does not exist. Indeed at $\eta^2 = 0$, χ^{-1} in the QPE phase is nonzero as we saw in Sec. IV. At $\eta^2 \neq 0$, growth of last term in Eq. (60) exceeds all bounds and cannot equate a constant term Ω_0^2 [notice that $D(\Delta)|_{\Delta=0} = 0$]. The inverse susceptibility therefore remains positive deep in the QPE phase with $\chi_{\min}^{-1} \neq 0$.

We note that when the temperature increases so that $\Delta \sim T$ and we are no longer in the QPE phase (red in Fig. 7), we enter the "tornado" region of the QCP influence (blue in Fig. 7) where $\chi^{-1} \sim \Delta^2 \sim T^2$, as was shown in Sec. IV. At this point the quadratic temperature dependence dominates and coupling to the acoustic phonons becomes negligible; as a result a turn-over in the inverse susceptibility from $-T^4$ to $+T^2$ dependence occurs (see Fig. 9).

E. Quantum critical temperature-dependent dielectric susceptibility

We already know that there exists a classical phase transition at T_c for $g < 0$ and $\eta = 0$; for $\eta \neq 0$ could this line of transitions enter the $g > 0$ part of the phase diagram and result in a reentrant quantum ferroelectric phase near the $g = 0$ QCP? In order to explore this possibility, we study the temperature-dependent susceptibility near the QCP (at $g = 0$) and find that unstable behavior is possible. Next we follow the line of transitions, where $\chi^{-1} = \Delta^2 = 0$ and show that its behavior is changed for $\eta > \eta_c$.

We begin with $\chi(T)$ in the vicinity in the quantum critical regime where $g = 0$ (trajectory 2 in Fig. 6); here $\Omega_0^2 = g = 0$ and $q \sim \omega \sim T \gtrsim 0$ at low temperatures. Taking $\eta = 0$, the spectral gap (59) becomes

$$\Delta_{\gamma_c}^2 = \frac{3\gamma_c}{2\pi^2} \int dq \, q n_B(q/T) \equiv \tilde{\alpha}\gamma_c T^2 = \frac{\gamma_c T^2}{4} \qquad (62)$$

and we recover the quadratic temperature dependence, $\chi_{\gamma_c}^{-1} = \Delta_{\gamma_c}^2 \sim T^2$, that was derived in Sec. IV B.

With $\eta \neq 0$, the η contribution to the gap becomes

$$\Delta_\eta^2 = -\frac{4\eta^2}{2\pi^2} \int dq \frac{q}{\tilde{c}^2 - 1} \left(n_B(q/T) - \frac{n_B(\tilde{c}q/T)}{\tilde{c}} \right) \equiv -\tilde{\beta}\eta^2 T^2.$$
$$\qquad (63)$$

For both cases $\tilde{c} \lesssim 1$, the expression under the integral in Eq. (63) is positive (see Appendix B for specifics), which results in a negative coefficient for Δ_η^2. Adding both γ_c and η terms in the gap Eq. (59), we write the expression for the dielectric susceptibility

$$\chi^{-1} = \Delta^2 = (\tilde{\alpha}\gamma_c - \tilde{\beta}\eta^2)T^2 = \left(\frac{\gamma_c}{4} - \tilde{\beta}\eta^2 \right)T^2, \qquad (64)$$

where $\tilde{\alpha}$ and $\tilde{\beta}$ are explicitly calculated in Appendix C. When the coefficient of T^2 is zero, namely, when

$$\eta = \eta_c = \sqrt{\frac{\gamma_c}{4\widetilde{\beta}}} = \sqrt{\frac{3}{4}\left(\frac{\widetilde{c}^3(\widetilde{c}^2-1)}{\widetilde{c}^3-1}\right)\gamma_c}, \qquad (65)$$

the phase boundary line ($\chi^{-1}=0$) becomes vertical in the approach to the QCP; when $\eta > \eta_c$, it "meanders" to the right leading to reentrant behavior.

F. Details of the phase boundary ($\chi^{-1}=0$)

We now follow the phase transition line, defined by $\chi^{-1} = 0$ ($\Delta = 0$) out to finite temperatures. From Sec. IV we know that there is a classical ferroelectric-paraelectric phase transition at $g < 0$ at Curie temperature $T_c(g)$; it is depicted as a solid line in Fig. 6, where the dielectric susceptibility diverges, $\chi = \Delta^{-2} \to \infty$. Our results in Sec. IV are for $\eta = 0$, and we study the effect of $\eta > \eta_c > 0$ on this transition line.

To do this, we look for a solution to the gap Eq. (59), when $\Delta(T_c, \eta) = 0$, which yields the transition line $T_c(g, \eta)$. When the spectral gap closes, the dispersion relations of the TO soft polarization and the LA acoustic modes both become linear [$\omega_p(q) = q$ and $\omega_a(q) = \widetilde{c}q$]. Inserting these values into Eq. (59) and setting $\Delta = 0$, we obtain

$$-2\pi^2\Omega_0^2 = 3\gamma_c\int_0^{q_{max}}dq\,qn_B(q/T_c)$$

$$-\frac{4\eta^2}{(\widetilde{c}^2-1)}\int_0^{q_{max}}dq\,q\left[n_B(q/T_c)-\frac{n_B(\widetilde{c}q/T_c)}{\widetilde{c}}\right]$$

$$=T_c^2\left\{3\gamma_c\int_0^{u_{max}}du\,un_B(u)\right.$$

$$\left.-\frac{4\eta^2}{(\widetilde{c}^2-1)}\int_0^{u_{max}}du\,u\left[n_B(u)-\frac{n_B(\widetilde{c}u)}{\widetilde{c}}\right]\right\} \quad (66)$$

for the equation determining $T_c(g)$. At low temperatures, we note that we recover the scaling relation $\Omega_0^2 = g \sim T_c^2$ since both integrals become proportional to T_c^2 ($u_{max} = \frac{q_{max}}{T_c} \gg 1$). At high temperatures $n_B(u) \approx \frac{1}{u}$, so the right-hand side of Eq. (66) becomes proportional to T_c, and we recover the classical behavior $g \sim T_c$.

Figure 10 shows the $T_c(g)$ transition line. For $\eta > \eta_c \approx 0.6$, the transition line "wanders" into the $g > 0$ region, leading to a reentrant quantum ferroelectric phase. Such reentrance suggests the possibility of nearby coexistence and a line of first-order transitions ending in a tricritical point, but the confirmation of this phase behavior requires a calculation beyond that presented here and will be the topic of future work.

In order to make direct comparison with experiment, we must now restore dimensions to our coupling constant and more generally to our Lagrangian (49). We start by explicitly restoring all physical coefficients to the Lagrangian as follows:

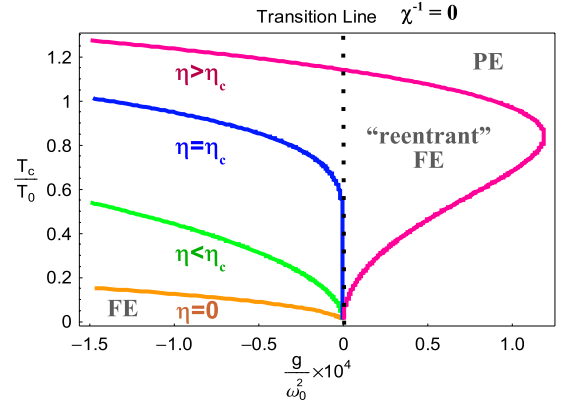$$\beta F = \int\frac{d^3\widetilde{x}d\tau}{\hbar}L,$$

FIG. 10. (Color online) The transition line $T_c(g)$ for different values of η, the acoustic coupling constant; for $\eta > \eta_c$ a reentrant quantum ferroelectric (FE) phase emerges. The phase boundaries result from numerical solution of the gap equation ($\Delta(\eta \neq 0) = 0$) discussed in the text; the parameters used here are as follows: $\gamma_c = 1$, $\widetilde{c} = 0.9$, $\eta_c = 0.62$, and $\{\eta > \eta_c, \eta < \eta_c\} = \{0.63, 0.59\}$.

$$L = \frac{\alpha}{2}[(\partial_\tau\widetilde{P})^2 + c_s^2(\nabla\widetilde{P})^2] + \frac{r_D}{2}\widetilde{P}^2 + \frac{\gamma_D}{4}\widetilde{P}^4$$

$$-\eta_D(\nabla\widetilde{\phi})\widetilde{P}^2 + \frac{\rho}{2}[(\partial_\tau\widetilde{\phi})^2 + c_a^2(\nabla\widetilde{\phi})^2], \qquad (67)$$

where c_s and c_a are the soft optical and acoustic phonon velocities, respectively, and where $\widetilde{P}$ and $\widetilde{\phi}$ are the unrescaled physical polarization and phonon displacement fields. Then by writing

$$\frac{\widetilde{x}}{c_s} = x, \quad \frac{c_s^3\alpha}{\hbar}\widetilde{P}^2 = P^2, \quad \frac{c_s^3\rho}{\hbar}\widetilde{\phi}^2 = \phi^2 \qquad (68)$$

we obtain Eq. (49), the rescaled Lagrangian,

$$\beta F = \int d^3\widetilde{x}d\tau\mathcal{L}_E(P,\phi),$$

$$\mathcal{L}_E(P,\phi) = \frac{1}{2}[(\partial_\tau P)^2 + (\nabla P)^2] + \frac{r}{2}P^2 + \frac{\gamma}{4}P^4$$

$$-\eta(\nabla\phi)P^2 + \frac{1}{2}[(\partial_\tau\phi)^2 + \widetilde{c}^2(\nabla\phi)^2], \quad (69)$$

where

$$\frac{c_s^2}{\hbar}L = \mathcal{L}_E, \quad r = \frac{r_D}{\alpha}, \quad \gamma = \frac{\hbar}{c_s^3\alpha^2}\gamma_D,$$

$$\eta = \frac{1}{\alpha c_s^{5/2}}\sqrt{\frac{\hbar}{\rho}}\eta_D, \quad \widetilde{c} = \frac{c_a}{c_s}. \qquad (70)$$

In the dimensionless units used in this section, we found that

$$\eta_c = \sqrt{\frac{\widetilde{\alpha}}{\widetilde{\beta}}}\gamma_c = \sqrt{\frac{3}{4}\left(\frac{\widetilde{c}^3(\widetilde{c}+1)}{\widetilde{c}^2+\widetilde{c}+1}\right)}\gamma_c, \qquad (71)$$

where $\widetilde{\alpha}=\frac{1}{4}$ and $\widetilde{\beta}=(\frac{\widetilde{c}^2+\widetilde{c}+1}{3\widetilde{c}^3(\widetilde{c}+1)})$. Using Eq. (70), we can now rewrite this critical coupling in dimensionful terms as follows:

$$\eta_{cD} = \sqrt{\frac{\rho}{\hbar}}\alpha c_s^{5/2}\eta_c = \sqrt{\frac{\rho}{\hbar}}\alpha c_s^{5/2}\sqrt{\frac{3}{4}\left(\frac{\widetilde{c}^3(\widetilde{c}+1)}{\widetilde{c}^2+\widetilde{c}+1}\right)}\sqrt{\frac{\hbar}{c_s^3\alpha^2}}\gamma_{cD}$$

$$= c_s\sqrt{\rho\gamma_{cD}}\sqrt{\frac{3}{4}\left(\frac{\widetilde{c}^3(\widetilde{c}+1)}{\widetilde{c}^2+\widetilde{c}+1}\right)}. \qquad (72)$$

For SrTiO$_3$, the acoustic[41,42] and the soft-mode[38] velocities have been measured to be $c_a \approx 8000$ m/s and $c_s \approx 10000$ m/, respectively, so that $\widetilde{c}=0.8$; the crystal mass density is 5.13 g/cm^3=5.13×10^3 kg/m^3. The value of γ_c has been measured[15,16] using ferroelectric Arrott plots of E/P vs P^2 to be $\epsilon_0\gamma_{cD}=0.2$ m^4/C^2. Inputting all these numbers and $\eta_c=0.6$ into our dimensionful expression for η_{cD}, we obtain

$$\eta_{cD}^{\text{STO}} = 5.74 \times 10^{10} \text{ Jm/C}^2 \qquad (73)$$

as the dimensionful critical coupling to be compared with experiment.

Next we estimate the experimental value of η in SrTiO$_3$ as[43] $\eta^{\text{STO}} \approx \frac{Q}{s}$ where Q and s are the typical magnitudes of the electrostrictive constants and the elastic compliances,[43,44] respectively; here we use the values[43] $Q=0.05$ m^4/C^2 and $s=3\times10^{-12}$ ms^2/kg. Therefore we obtain

$$\eta_{\text{STO}} = 1.7 \times 10^{10} \text{ Jm/C}^2 \qquad (74)$$

so that from our analysis we observe that $\eta_{\text{STO}} < \eta_{cD}^{\text{STO}}$ for the SrTiO$_3$ system. However, there are two points of uncertainty here that we should emphasize: (i) we use experimental values for SrTi^{16}O$_3$ as they are not yet available for SrTi^{18}O$_3$; (ii) we use values of Q and s at room temperature, and these quantities need to be determined at low temperatures. Despite the roughness of our estimate, it is reasonable to assume η is not changed dramatically by the issues raised in (i) and (ii). We encourage further experimental investigations of SrTi^{18}O$_3$ at low temperatures to clarify this situation.

G. Translational invariance as protection against damping effects and singular interactions

Our analysis of the effects of acoustic coupling has been limited to a Hartree treatment of the leading self-energy. This approach neglects two physical effects: (i) damping, the process by which a soft-mode phonon can decay by the emission of an acoustic phonon and (ii) the possibility of singular interactions induced by the exchange of acoustic phonons

Similar issues are of great importance in magnetic quantum phase transitions in metals, where the coupling of the magnetization to the particle-hole continuum of electrons introduces damping.[45–47] For example, in the simplest Hertz-Moriya treatment of a ferromagnetic quantum critical point, damping by the electron gas gives rise to a quadratic Lagrangian of the form

$$S_M = \sum_{q,\nu}\left[q^2 + r + \frac{|\nu|}{q}\right]|M(q,\nu)|^2, \qquad (75)$$

where the term linear in $|\nu|$ is a consequence of damping by the particle-hole continuum. This term plays a vital role in the quantum critical behavior; by comparing the dimensions of the q^2 term with the damping term, we see that $[\nu]\equiv q^3$, which means that the temporal dimension scales as $z=3$ spatial dimensions under the renormalization group. This has the effect of pushing the upper critical dimension down from $4-1=3$ to $4-z=1$ dimensions. In addition to this effect, the coupling to the electron-hole continuum also introduces non-local interactions between the magnetization modes, casting doubt on the mapping to a ϕ^4 field theory.

Fortunately, translational invariance protects the ferro-electric against these difficulties. Translational invariance guarantees that the soft mode cannot couple directly to the displacement of the lattice; instead it couples to the strain, the gradient of the displacement, according to the interaction $H_I=-\eta\nabla\phi P^2$. When we integrate out the acoustic phonons, the induced interaction between the soft-mode phonons takes the form

$$V(q,\nu) = -4\eta^2\frac{q^2}{\nu^2+\widetilde{c}^2q^2}, \qquad (76)$$

where the numerator results from the coupling to the strain, rather than the displacement. The presence of the q^2 term in the numerator removes the "Coulomb-type" $1/q^2$ divergence at small q, protecting the soft-mode interactions from the development of a singular long range component.

A similar effect takes place with the damping. To see this, we need to examine the imaginary part of the self-energy appearing in the Gaussian contribution to action (23),

$$S_G = \sum_{q,\nu}\frac{1}{2}[\nu^2 + q^2 + r + \Sigma_\eta(q)]|P(\vec{q},\nu)|^2. \qquad (77)$$

Damping results from the imaginary part of self-energy, $\Sigma_n''(q,\omega)$. To compute the damping, we generalize Σ_η given in Eq. (57) to finite frequency, obtaining

$$\Sigma_\eta(q,z) = 2\eta^2\int\frac{d^3k}{(2\pi)^3}k^2\left\{\frac{\left[n_p+\frac{1}{2}\right]}{\omega_p[(z-\omega_p)^2-\omega_a^2]}\right.$$

$$\left.+\frac{\left[n_a+\frac{1}{2}\right]}{\omega_a[(z-\omega_a)^2-\omega_p^2]}+(z\leftrightarrow-z)\right\}, \qquad (78)$$

where we have used the short-hand $\omega_a\equiv\omega_a(k)$, $\omega_p\equiv\omega_p(\vec{q}-\vec{k})$, $n_a=n_B[\omega_a(k)]$, and $n_p=n_B[\omega_p(\vec{q}-\vec{k})]$. The imaginary part of this expression at zero temperature, for positive ν, is then given by

$$\text{Im}[\Sigma_\eta(q, \nu - i\delta)] = \pi \eta^2 \int \frac{d^3k}{(2\pi)^3} \frac{k^2}{\omega_p \omega_a} \delta(\omega - \omega_a - \omega_p).$$

(79)

We can determine the small q, ω behavior of this damping rate by simple dimensional analysis. The dimension of the right-hand side is $[q^5]/[\omega^2] \sim q^2$, so the damping rate must have the form

$$\text{Im}\,\Sigma(q,\nu) \sim \eta^2 \nu^2 F\left(\frac{q}{|\nu|}, \frac{\Delta}{|\nu|}\right),$$

(80)

where a more careful analysis of the integral reveals that $F(\frac{q}{|\nu|}, \frac{\Delta}{|\nu|})$ is not singular at either small momentum or frequency. The most important aspect of this result is that the scattering phase space grows quadratically with frequency and momentum, so that it does not dominate over the other terms in action (77). The scaling dimension of frequency remains the same as that of momentum, and thus the upper-critical spatial dimension remains as $d=3$.

VI. DISCUSSION

A. Logs, dipolar interactions, and the Barrett formula

Before summarizing our results, let us briefly touch on a number of topics closely related to our work which we have not yet discussed; more specifically they include logarithmic corrections in the upper critical dimension, dipolar interactions, and the use of the Barrett formula for quantum paraelectrics. As we have already noted in Sec. V B, the polarization mode-mode interaction γ_c and coupling to the acoustic phonons η are both marginally relevant in the dimension of physical interest $d=3$. Thus logarithmic corrections to the scaling relations (Sec. III) have to be included; we have already seen their appearance in the expression for α_3 in Eq. (44). The correction to scaling of the free energy near the classical ferroparaelectric phase transition in four dimensions is[1]

$$f_{\text{cl}}(t, \gamma_c) = f_0(t, \gamma_c)[1 + 9\gamma_c \ln(t_0/t)]^{1/3},$$

(81)

where $t = \left|\frac{T - T_c}{T_c}\right|$ is the reduced temperature, $f_0(t, \gamma_c) = t^2 \Phi\left(\frac{E/E_0}{|t/t_0|^{3/2}}\right)$ is the scaling form of the free energy with a universal scaling function Φ, t_0 is the reduced Debye temperature for the soft mode (48) and γ_c is the polarization mode-mode coupling at QCP. Since $\chi = \frac{\partial^2 f}{\partial E^2}|_{E=0}$, we have

$$\chi = \chi_0[1 + 9\gamma_c \ln(t_0/t)]^{1/3},$$

(82)

where $\chi_0 \sim t^{-1}$. By applying the quantum-classical analogy (Sec. III), we write at the upper critical dimension, $d_c^u = 3$ ($d + z = 4$; $z = 1$),

$$f_{qm}(g, \gamma_c) = f_0(g, \gamma_c)[1 + 9\gamma_c \ln(g_0/g)]^{1/3},$$

(83)

where $g_0 \equiv \omega_0^2$ is the Debye frequency for the soft mode squared, $f_0(g, \gamma_c)$ has the same form as before, and g is the tuning parameter. By setting $\chi = \frac{\partial^2 f}{\partial E^2}|_{E=0}$, the dielectric susceptibility becomes

$$\chi = \chi_0[1 + 9\gamma_c \ln(g_0/g)]^{1/3},$$

(84)

where $\chi_0 \sim g^{-1} \sim T^{-2}$. The temperature dependence of χ with logarithmic corrections is then found by making the substitution $g \sim T^2$ in Eq. (84), and these results are identical to those found previously using diagrammatic techniques.[17] An analogous procedure can be used to find the logarithmic corrections to other thermodynamic quantities.

We note that here we assume the upper critical (spatial) dimension $d_c^u = 3$; however if we include uniaxial dipole-dipole interactions, we will have $d_c^u = 2$. Basically this is because when all dipoles point in the (same) z direction, the TO polarization frequency (26) becomes[48]

$$\omega^2(q) = q^2 + \Delta^2 + \beta \frac{q_z^2}{q^2},$$

(85)

where β is a constant, and we derive Eq. (85) in Appendix D. We note that the last term of Eq. (85) is specific to the uniaxial (e.g., tetragonal) case and is not present for isotropic dipolar interactions. Applying simple scaling, we obtain

$$\tilde{q}_{x(y)} = \frac{q_{x(y)}}{b}, \quad \tilde{q}_z = \frac{q_z}{b^k},$$

(86)

where the constants $b, b^k > 1$ represent flow to the infrared (IR) limit of the QCP. We show in Appendix D that in order for Eqs. (85) and (86) to be satisfied simultaneously, k must equal 2 so that q_z "counts" for effectively *two* dimensions ($d_{\text{eff}}^{\text{space}} = d + 1$), so that for a quantum uniaxial ferroelectric the total effective dimension is $d_{\text{eff}} = d_{\text{eff}}^{\text{space}} + z = (d+1) + z = d+2$ with $d_c^u = 2$ since then we obtain $d_{\text{eff}} = 4$.

At this time, it is not known whether SrTi^{18}O$_3$ is cubic or tetragonal at low temperatures. In any case, we expect the samples under study to be structurally multidomain so that averaging over long length scales will make them effectively cubic; thus uniaxial dipolar interactions do not need to be considered. The observed T^2 behavior of χ in the vicinity of the QCP supports this contention (i.e., $d_{\text{eff}}^{\text{space}} = 3$); for $d_{\text{eff}}^{\text{space}} = 4$, a different T dependence ($\chi^{-1} \sim T^3$) is expected[21] for a QPE so that a reexamination of the underlying model would be necessary to match experiment. Until details of the samples are known, this situation cannot be ascertained. We note that such T^2 dependence of the inverse susceptibility has also been observed[25] in mixed crystal ferroelectrics KTa$_{1-x}$Nb$_x$O$_3$ and Ka$_{1-y}$Na$_y$TaO$_3$ where uniaxial dipolar interactions are not important, and we encourage further low-temperature studies of these systems.

A consistent discrepancy between the observed low-temperature dielectric susceptibility and the Barrett formula[37] has been observed in the quantum paraelectric phase.[25,31] Here we emphasize that the discrepancy occurs when the system gets very close to the QCP; thus it provides a measure of the tuning distance to the QCP. Because the optical polarization mode softens as the system approaches the QCP, with the gap vanishing completely here, the momentum dependence in the dispersion relation (26) becomes important. It is exactly for this reason that the Barrett formula, which assumes a constant dispersion relation, $\omega = \tilde{\omega}_0$, breaks down close to the QCP.

The Barrett formula[37] works well deep in the QPE phase (Sec. V D), where the gap is much bigger than temperature. One such example is $KTaO_3$ (KTO), which remains paraelectric down to zero temperature, but in contrast to $SrTiO_3$ (STO) shows a much lower value of the zero-temperature dielectric susceptibility ($\chi_{KTO} \approx 4000$, $\chi_{STO} \approx 24\,000$).[31,49] The closer the system is tuned to the QCP, the smaller the spectral gap and the bigger the dielectric susceptibility. Therefore, STO sits much closer to the QCP than KTO, and indeed KTO shows a nice fit to the Barrett formula.[49] Notice that by plugging $\widetilde{\omega}_0$ into Eq. (33), we get the Barrett expression,

$$\chi^{-1} = \Delta^2 = \Omega_0^2 + \frac{3\gamma_c}{4\pi^2}\left(\frac{\coth(\widetilde{\omega}_0/2T)}{\widetilde{\omega}_0}q_{max}^3 - \frac{q_{max}^2}{2}\right)$$

$$= \frac{1}{M}\left(\frac{T_1}{2}\coth(T_1/2T) - T_0\right), \tag{87}$$

where $T_1 \equiv \widetilde{\omega}_0$, and M and T_0 are fitting constants.

B. Summary and open questions

Let us now summarize the main results of the paper. Here our aim has been to characterize the finite-temperature properties of a material close to its quantum ferroelectric critical point; we have rederived and extended previous theoretical results using scaling methods and self-consistent Hartree theory. In the process we have made an analogy between temperature as a boundary effect in time and the Casimir effect, and have used this to shed light on both problems. Using simple finite-size scaling, we have presented straightforward derivations of finite-temperature observables for direct comparison with experiment, and our approach has yielded a scaling form $\chi(\omega) = \frac{1}{\omega}F(\frac{\omega}{T})$ which serves as an additional probe of T_0, the soft-mode Debye temperature scale where we expect crossover between Curie (T) and quantum critical (T^2) behavior in χ^{-1}. We emphasize that this scaling method is useful in this system where z is low ($z=1$); otherwise if z is higher, the system is usually well above its upper critical dimension where this approach is inappropriate. Next we have used self-consistent Hartree methods to determine the $T-g$ phase diagram and the crossover between classical and quantum behavior. In particular we see the influence of the quantum critical point on the susceptibility at finite temperatures, and we can put in materials parameters to determine the size of its basin of attraction. Finally we include coupling to an acoustic phonon and find that it affects the transition line; for such couplings greater than a threshold strength there is a reentrant quantum ferroelectric phase.

Naturally these results suggest a number of open questions and here we list a few:

(i) The presence of a reentrant phase suggests the possibility of nearby phase coexistence, a tricritical point, and a line of first-order transitions. This is a particularly appealing scenario given that recent experiments[50] suggest coexistence of QPE and QFE in $SrTi^{18}O_3$ and is a topic we plan to pursue shortly.

(ii) If indeed there is a tricritical point and a line of first-order phase transitions, could there also be a metaelectric critical point in the $g-E$ plane analogous to the metamagnetic situation[51,52] in some metallic systems? There is indication that an analogous metaelectric critical point occurs in a multiferroic system,[53] so this is a question driven by recent experiment.

(iii) What happens when we add spins to a system near its quantum ferroelectric critical point? Would the resulting multiferroic have particularly distinctive properties?

(iv) Similarly, what type of behavior do we expect if we dope a quantum parelectric in the vicinity of a QCP? There is by now an extensive body of evidence that electronically mediated superconductivity is driven by the vicinity to a magnetic quantum critical point, a phenomenon of "avoided criticality," whereby superconductivity is in the vicinity of a naked magnetic quantum critical point.[54,55] In such systems, the metallic transport properties develop strange metallic properties that have been termed "non-Fermi-liquid behavior."[56,57] This raises the important question, as to what, if any, is the ferroelectric counterpart to this behavior? In particular, how does the presence of a soft mode affect the semimetallic properties of a doped quantum critical ferroelectric, and does a doped ferroelectric quantum critical point also develop superconductivity via the mechanism of avoided criticality?

We believe that we have only begun to explore the rich physics associated with the quantum ferroelectric critical point, a simple setting for studying many issues associated with quantum criticality that emerge in much more complex materials. Furthermore the possibility of detailed interplay between theory and experiment is very encouraging.

APPENDIX A: $D(\Delta)$ AND $A(\eta)$

We derive expressions for $D(\Delta)$ and $A(\eta)$ [Eq. (61)] using the gap Eq. (59) deep in the QPE region (D), where $g \gg 0$ and $\Delta \gg T \approx 0$. Collecting all "$\frac{1}{2}$" terms under integrals of $\Delta_{\gamma_c}^2$ and Δ_η^2 in Eq. (59), we obtain the expression for $D(\Delta)$,

$$D(\Delta) \equiv \frac{3}{2}\gamma_c \int \frac{d^3q}{(2\pi)^3}\left(\frac{1}{\omega_p} - \frac{1}{q}\right)$$

$$- 2\eta^2 \int \frac{d^3q}{(2\pi)^3}q^2\left(\frac{1}{\omega_a[\omega_p^2 - \omega_a^2]} - \frac{1}{q^3\widetilde{c}[1 - \widetilde{c}^2]}\right)$$

$$- 2\eta^2 \int \frac{d^3q}{(2\pi)^3}q^2\left(\frac{1}{\omega_p[\omega_a^2 - \omega_p^2]} - \frac{1}{q^3[\widetilde{c}^2 - 1]}\right)$$

$$\equiv \frac{3\gamma_c}{4\pi^2}I_1 - \frac{\eta^2}{\widetilde{c}\pi^2}I_2 - \frac{\eta^2}{\pi^2}I_3,$$

$$I_1 = \int_0^{q_{max}} dq \, q^2 \left(\frac{1}{\sqrt{\Delta^2 + q^2}} - \frac{1}{q} \right),$$

$$I_2 = \int_0^{q_{max}} dq \, q^3 \left(\frac{1}{\Delta^2 + q^2[1 - \tilde{c}^2]} - \frac{1}{q^2[1 - \tilde{c}^2]} \right),$$

$$I_3 = \int_0^{q_{max}} dq \, q^4 \left(\frac{1}{\sqrt{\Delta^2 + q^2}[-\Delta^2 + q^2(\tilde{c}^2 - 1)]} - \frac{1}{q^3[\tilde{c}^2 - 1]} \right).$$
(A1)

Notice that $\lim_{\Delta \to 0} D(\Delta) = 0$, since all three integrals I_1, I_2, and I_3 become zero at zero gap. We split the integrals I_i ($i = 1, 2, 3$) into two parts, $I_i = \int_0^{n\Delta} + \int_{n\Delta}^{q_{max}}$, where $n\Delta \gg \Delta$. Since $q \gg \Delta$ in the second integral part, we neglect its Δ dependence and get a zero contribution. Thus, only the first integral part contributes, and $D(\Delta)$ becomes a function of Δ only, with no temperature dependence.

Next we show that the second Bose-Einstein $n_B[\omega_a(q)]$ term under the integral of Δ_η^2 in Eq. (59) results in the form $A(\eta)$ in Eq. (61),

$$-4\eta^2 \int \frac{d^3q}{(2\pi)^3} q^2 \frac{n_B[\omega_a(q)]}{\omega_a[\omega_p^2 - \omega_a^2]}$$

$$= -4\eta^2 \int \frac{d^3q}{(2\pi)^3} q^2 \frac{n_B[\omega_a(q)]}{\tilde{c}q[\Delta^2 + q^2(1 - \tilde{c}^2)]}$$

$$\approx -\frac{4\eta^2}{\tilde{c}} \frac{T^4}{\Delta^2} \int \frac{d^3u}{(2\pi)^3} u n_B(\tilde{c}u) \equiv -A(\eta) \frac{T^4}{\Delta^2}, \quad (A2)$$

where $u = q/T$. Notice that we approximate $\Delta^2 \gg q^2(1 - \tilde{c}^2)$ in the second line of Eq. (A2). For low momenta, this is indeed the case. For large momenta, $q \gg \Delta \gg T \approx 0$, we neglect Δ in Eq. (A2) and the integral becomes

$$-\frac{4\eta^2}{2\pi^2 \tilde{c}(1 - \tilde{c}^2)} \int dq \, q n_B(\tilde{c}q).$$
(A3)

In the limit $q \gg T$, $n_B(\tilde{c}q) \approx e^{-\tilde{c}q/T}$ and Eq. (A3) becomes exponentially small ($\sim T^2 e^{-\tilde{c}q/T}$) and can be neglected. Similarly, we neglect the rest of the terms in the gap function (59) with Bose-Einstein thermal distribution $n_B[\omega_p(q)]$. Deep in the QPE phase $\Delta \gg T$, so that $n_B[\omega_p(q)] \approx e^{-\Delta/T}$ at low momenta, or $n_B[\omega_p(q)] \approx e^{-q_{large}/T}$ at large momenta. In both cases $\Delta, q_{large} \gg T$, the integrals containing $n_B[\omega_p(q)]$ become exponentially small and so are negligible.

APPENDIX B: INTEGRAL (63) IS POSITIVE FOR $\tilde{c} \lesssim 1$

We also show that the expression under the integral in Eq. (63) is positive for the two cases, $\tilde{c} \lesssim 1$. First, assuming that $\tilde{c} < 1$, $\tilde{c}q < q$ (positive q's) and $n_B(\tilde{c}/T) > n_B(q/T)$ we write

$$\left\{ n_B(q/T) - \frac{n_B(\tilde{c}q/T)}{\tilde{c}} \right\} \frac{1}{\tilde{c}^2 - 1} > \left(1 - \frac{1}{\tilde{c}} \right) n_B(\tilde{c}q/T) \frac{1}{\tilde{c}^2 - 1}$$

$$= \frac{1}{\tilde{c}(\tilde{c} + 1)} n_B(\tilde{c}q/T) \geq 0,$$
(B1)

which we note is positive. Similarly, for $\tilde{c} > 1$, $\tilde{c}q > q$, and $n_B(\tilde{c}q/T) < n_B(q/T)$, we write

$$\left\{ n_B(q/T) - \frac{n_B(\tilde{c}q/T)}{\tilde{c}} \right\} \frac{1}{\tilde{c}^2 - 1} > \left(1 - \frac{1}{\tilde{c}} \right) n_B(q/T) \frac{1}{\tilde{c}^2 - 1}$$

$$= \frac{1}{\tilde{c}(\tilde{c} + 1)} n_B(q/T) \geq 0 \quad (B2)$$

which is also positive. Therefore the integral in Eq. (63) is positive in both cases.

APPENDIX C: $\tilde{\alpha}$ AND $\tilde{\beta}$ ARE CONSTANTS

To evaluate the quantities $\tilde{\alpha}$ and $\tilde{\beta}$ in Eqs. (62) and (63), we make a change of variables to $u = q/T$, and $u = \tilde{c}q/T$, respectively. The expressions for these two constants then become

$$\tilde{\alpha} = \frac{3}{2\pi^2} \int_0^{q_{max}/T} du \, u n_B(u) = \frac{1}{4},$$

$$\tilde{\beta} = \frac{2}{\pi^2(\tilde{c}^2 - 1)} \left[\int_0^{q_{max}/T} - \frac{1}{\tilde{c}^3} \int_0^{\tilde{c}q_{max}/T} \right] du \, u n_B(u)$$

$$= \frac{1}{3(\tilde{c}^2 - 1)} \left(1 - \frac{1}{\tilde{c}^3} \right),$$
(C1)

where we have taken the limits of integration to infinity and used the result $\int_0^\infty du \, u n_B(u) = \frac{\pi^2}{6}$.

APPENDIX D: DIPOLE-DIPOLE INTERACTIONS IN UNIAXIAL FERROELECTRICS

The interaction energy between two dipoles $\vec{p}_i$ and $\vec{p}_j$ sitting on two sites $\vec{r}_i$ and $\vec{r}_j$, respectively, is

$$W_{ij}(\vec{r}) = \frac{\vec{p}_i \cdot \vec{p}_j - 3(\vec{n} \cdot \vec{p}_i)(\vec{n} \cdot \vec{p}_j)}{4\pi\epsilon_0 |\vec{r}|^3},$$
(D1)

where $\vec{n}$ is a unit vector in the direction of the vector $\vec{r} \equiv \vec{r}_j - \vec{r}_i$. From Eq. (D1), we find the total dipole-dipole interaction potential to be

$$W(\vec{r}) = \frac{1}{4\pi\epsilon_0} \sum_{i,j,a,b} p_i^a p_j^b \left(\frac{\delta_{ab}}{r^3} - \frac{3r^a r^b}{r^5} \right),$$
(D2)

where $r \equiv |\vec{r}|$, and a, b label vector coordinates. After we perform a Fourier transform, the interaction potential becomes

$$W(\vec{q}) = \frac{1}{\epsilon_0} \sum_{a,b} p_{\vec{q}}^a p_{-\vec{q}}^b \frac{q_a q_b}{q^2},$$
(D3)

where $q \equiv |\vec{q}|$ refers to the momentum dependence of $W(\vec{q})$. Assuming that all dipoles point in the same (z) direction in

the uniaxial case, we find that the dipole potential

$$W(\vec{q}) \sim \frac{q_z^2}{q^2}.$$ (D4)

$W(\vec{q})$ contributes to Lagrangian (49), $L_E[P,\Phi] \to L_E[P,\Phi] + W$, so that the TO polarization frequency (26) then reads[48]

$$\omega^2(q) = c_s^2 q^2 + \Delta^2 + \beta \frac{q_z^2}{q^2},$$ (D5)

where we introduce constant of proportionality β.

We show that Eqs. (85) and (86) leads to the condition $k=2$. Let us assume that $k>1$. Then

$$\tilde{q}^2 = \tilde{q}_x^2 + \tilde{q}_y^2 + \tilde{q}_z^2 = \frac{q_x^2 + q_y^2}{b^2} + \frac{q_z^2}{(b^2)^k} \approx \frac{q^2}{b^2},$$

$$\frac{\tilde{q}_z^2}{\tilde{q}^2} \approx b^{2-2k} \frac{q_z^2}{q^2}.$$ (D6)

Since we also rescale frequency $\omega(q)$ [Eq. (85)] by a constant, expressions $\tilde{q}^2$ and $\frac{\tilde{q}_z^2}{\tilde{q}^2}$ are to be proportional. This leads then to the condition

$$k = 2.$$ (D7)

[1] J. Cardy, *Scaling and Renormalization in Statistical Physics* (Cambridge University Press, Cambridge, 1999).

[2] S. L. Sondhi, S. M. Girvan, J. P. Carini, and D. Shahar, Rev. Mod. Phys. **69**, 315 (1997).

[3] S. Sachdev, *Quantum Phase Transitions* (Cambridge University Press, Cambridge, 1999).

[4] M. A. Continentino, *Quantum Scaling in Many-Body Systems* (World Scientific, Singapore, 2001).

[5] P. Coleman and A. J. Schofield, Nature (London) **433**, 226 (2005).

[6] H. B. G. Casimir, Proc. K. Ned. Akad. Wet. **51**, 793 (1948); H. B. G. Casimir and D. Polder, Phys. Rev. **73**, 360 (1948).

[7] M. Krech, *The Casimir Effect in Critical Systems* (World Scientific, Singapore, 1994).

[8] M. Kardar and R. Golestanian, Rev. Mod. Phys. **71**, 1233 (1999).

[9] S. K. Lamoreaux, Phys. Rev. Lett. **78**, 5 (1997).

[10] U. Mohideen and A. Roy, Phys. Rev. Lett. **81**, 4549 (1998).

[11] H. B. Chan, V. A. Aksyuk, R. N. Kleiman, D. J. Bishop, and F. Capasso, Science **291**, 1941 (2001).

[12] M. Lisanti, D. Iannuzzi, and F. Capasso, Proc. Natl. Acad. Sci. U.S.A. **102**, 11989 (2005).

[13] J. M. Obrecht, R. J. Wild, M. Antezza, L. P. Pitaevskii, S. Stringari, and E. A. Cornell, Phys. Rev. Lett. **98**, 063201 (2007).

[14] E. L. Venturini, G. A. Samura, M. Itoh, and R. Wang, Phys. Rev. B **69**, 184105 (2004).

[15] P. Coleman, Physica B **378-380**, 1160 (2006).

[16] S. E. Rowley, L. J. Spalek, and S. S. Saxena (unpublished); S. E. Rowley and S. S. Saxena (private communication).

[17] A. B. Rechester, Sov. Phys. JETP **33**, 423 (1971).

[18] D. E. Khmelnitskii and V. L. Shneerson, Sov. Phys. Solid State **13**, 687 (1971); Sov. Phys. JETP **37**, 164 (1973).

[19] R. Roussev and A. J. Millis, Phys. Rev. B **67**, 014105 (2003).

[20] N. Das and S. G. Mishra, arXiv:0707.2634 (unpublished).

[21] T. Schneider, H. Beck, and E. Stoll, Phys. Rev. B **13**, 1123 (1976).

[22] D. Schmeltzer, Phys. Rev. B **28**, 459 (1983).

[23] S. Sachdev, Phys. Rev. B **55**, 142 (1997).

[24] J. Hertz, Phys. Rev. B **14**, 1165 (1976).

[25] D. Rytz, U. T. Hochli, and H. Bilz, Phys. Rev. B **22**, 359 (1980).

[26] M. E. Fisher and P. G. deGennes, C. R. Seances Acad. Sci., Ser. B **287**, 207 (1978).

[27] D. M. Danchev, J. G. Brankov, and N. S. Tonchev, *Theory of Critical Phenomena in Finite-Size Systems: Scaling and Quantum Effects* (World Scientific, Singapore, 2000).

[28] E. Brezin and J. Zinn-Justin, Nucl. Phys. B **257**, 867 (1985).

[29] J. Rudnick, H. Guo, and D. Jasnow, J. Stat. Phys. **41**, 353 (1985).

[30] H. Chamati, D. M. Danchev, and N. S. Tonchev, Eur. Phys. J. B **14**, 307 (2000).

[31] K. A. Muller and H. Burkard, Phys. Rev. B **19**, 3593 (1979).

[32] M. E. Lines and A. M. Glass, *Principles and Applications of Ferroelectrics and Related Materials* (Oxford University Press, Oxford, 1977).

[33] R. Wang and M. Itoh, Phys. Rev. B **64**, 174104 (2001).

[34] M. C. Aronson, R. Osborn, R. A. Robinson, J. W. Lynn, R. Chau, C. L. Seaman, and M. B. Maple, Phys. Rev. Lett. **75**, 725 (1995).

[35] A. Schröder, G. Aeppli, R. Coldea, M. Adams, O. Stockert, H. von Löhneysen, E. Bucher, R. Ramazashvili, and P. Coleman, Nature (London) **407**, 351 (2000).

[36] T. Moriya, *Spin Fluctuations in Itinerant Electron Magnets* (Springer-Verlag, Berlin, 1985).

[37] J. H. Barrett, Phys. Rev. **86**, 118 (1952).

[38] Y. Yamada and G. Shirane, J. Phys. Soc. Jpn. **26**, 396 (1957).

[39] J. H. Haeni, P. Irvin, W. Chang, R. Uecker, P. Reiche, Y. L. Li, S. Choudhury, W. Tian, M. E. Hawley, B. Craigo, A. K. Tagantsev, X. Q. Pan, S. K. Streiffer, L. Q. Chen, S. W. Kirchoefer, J. Levy, and D. G. Schlom, Nature (London) **430**, 758 (2004).

[40] M. Takesada, M. Itoh, and T. Yagi, Phys. Rev. Lett. **96**, 227602 (2006).

[41] C. v. Korff Schmising, M. Bargheer, M. Kiel, N. Zhavoronkov, M. Woerner, T. Elsaesser, I. Vrejoiu, D. Hesse, and M. Alexe, Phys. Rev. B **73**, 212202 (2006).

[42] R. O. Bell and G. Rupprecht, Phys. Rev. **129**, 90 (1963).

[43] L. Palova, P. Chandra, and K. M. Rabe, Phys. Rev. B **76**, 014112 (2007).

[44] N. A. Pertsev, A. G. Zembilgotov, and A. K. Tagantsev, Phys. Rev. Lett. **80**, 1988 (1998).

[45] T. Moriya and A. Kawabata, J. Phys. Soc. Jpn. **34**, 639 (1973); **35**, 669 (1973).

[46] J. A. Hertz, Phys. Rev. B **14**, 1165 (1976).

[47] A. J. Millis, Phys. Rev. B **48**, 7183 (1993).

[48] A. I. Larkin and D. E. Khmel'nitskii, Sov. Phys. JETP **29**, 1123

(1969).

[49] A. R. Akbarzadeh, L. Bellaiche, K. Leung, J. Iniguez, and D. Vanderbilt, Phys. Rev. B **70**, 054103 (2004).

[50] H. Taniguchi, M. Itoh, and T. Yagi, Phys. Rev. Lett. **99**, 017602 (2007).

[51] A. J. Millis, A. J. Schofield, G. G. Lonzarich, and S. A. Grigera, Phys. Rev. Lett. **88**, 217204 (2002).

[52] P. Gegenwart, Q. Si, and F. Steglich, Nat. Phys. **4**, 186 (2008).

[53] J. W. Kim *et al.* (unpublished).

[54] N. D. Mathur, F. M. Grosche, S. R. Julian, I. R. Walker, D. M. Freye, R. K. W. Haselwimmer, and G. G. Lonzarich, Nature (London) **394**, 39 (1998).

[55] R. B. Laughlin, G. G. Lonzarich, P. Monthoux, and D. Pines, Adv. Phys. **50**, 361 (2001).

[56] P. Coleman, C. Pepin, Q. Si, and R. Ramazashvili, J. Phys.: Condens. Matter **13**, R723 (2001).

[57] H. von Löhneysen, A. Rosch, M. Vojta, and P. Wölfle, Rev. Mod. Phys. **79**, 1015 (2007).